Structural Hierarchy in Molecular Films of Two Class II Hydrophobins†

Arja Paananen,‡ Elina Vuorimaa,§ Mika Torkkeli,|| Merja Penttilä,‡ Martti Kauranen,⊥ Olli Ikkala,# Helge Lemmetyinen,§ Ritva Serimaa,|| and Markus B. Linder*,‡

VTT Biotechnology, Technical Research Centre of Finland, P.O. Box 1500, FIN-02044 VTT, Espoo, Finland; Institute of Materials Chemistry, P.O. Box 541, and Department of Physics, Tampere University of Technology, FIN-33101 Tampere, Finland; Department of Physical Sciences, University of Helsinki, FIN-00014 Helsinki, Finland; and Department of Engineering, Physics, and Mathematics, Helsinki University of Technology, P.O. Box 2200, FIN-02015 HUT, Espoo, Finland

Received January 9, 2003; Revised Manuscript Received March 12, 2003

ABSTRACT: Hydrophobins are highly surface-active proteins that are specific to filamentous fungi. They function as coatings on various fungal structures, enable aerial growth of hyphae, and facilitate attachment to surfaces. Little is known about their structures and structure−function relationships. In this work we show highly organized surface layers of hydrophobins, representing the most detailed structural study of hydrophobin films so far. Langmuir−Blodgett films of class II hydrophobins HFBI and HFBII from *Trichoderma reesei* were prepared and analyzed by atomic force microscopy. The films showed highly ordered two-dimensional crystalline structures. By combining our recent results on small-angle X-ray scattering of hydrophobin solutions, we found that the unit cells in the films have dimensions similar to those of tetrameric aggregates found in solutions. Further analysis leads to a model in which the building blocks of the two-dimensional crystals are shape-persistent supramolecules consisting of four hydrophobin molecules. The results also indicate functional and structural differences between HFBI and HFBII that help to explain differences in their properties. The possibility that the highly organized surface assemblies of hydrophobins could allow a route for manufacturing functional surfaces is suggested.

Hydrophobins are surface-active proteins produced and so far only observed in filamentous fungi. They have roles important to growth and morphology and act, for example, as coatings on the surface of spores, fruiting bodies, and mycelium; they are also found secreted into the surroundings (*1*, *2*). Mutant phenotypes lacking hydrophobin genes are more easily wetted and have been shown to have impaired growth of aerial hyphae (*3*, *4*). The high surface activity of the hydrophobin protein (*2*) is likely to be the reason for their importance in growth, and especially for penetrating the air−water interface. Also, the coatings formed by hydrophobins probably serve to protect aerial structures. Pathogenic fungi also rely on the surface-active properties of hydrophobins for attachment to their hosts, for example, on insect cuticles or plant leaves (*5*).

Hydrophobins contain eight characteristic Cys residues that through four disulfide bridges have been suggested to form four loops in the polypeptide chain, appearing as pairs near both chain ends (*2*, *6*). This motif is expected to play a role in their biological functions, but at the level of molecular structure very little is understood about the properties of hydrophobins. Despite the low sequence identity, hydropathy plots can be used to group them into classes I and II (*7*). All published data so far support the postulate that the main functional difference between the two classes is in the solubility of their aggregates, where the detailed structure of the loops may play an essential role. Nonetheless, the two classes clearly share features, such as surface adhesion and surface activity, which suggests that their biological function depends on surface activity and self-assembly.

A representative of class I is the SC3 hydrophobin from *Schizophyllum commune*, which upon solvent drying or bubbling forms random patterns of nanoscopic rodlets and their bundles on surfaces (*8*−*11*). The rodlets (widths ca. 5 nm and lengths ca. 20 nm) are highly insoluble and are apparently related to amyloid fibrils (*9*, *12*, *13*).

Much-studied examples of class II hydrophobins are HFBI and HFBII from *Trichoderma reesei* (see ref *14* for a comparison of their sequences). They are very soluble in water and form tetramers at high concentrations of 10 mg/mL; at lower concentrations, monomers and dimers were also observed (*15*). When solutions of HFBI and HFBII are shaken, they self-assemble rapidly to form solid fibrillar aggregates. Upon standing, the solutions form fibrils more slowly. In contrast to the nanoscale rodlets, such class II fibrils can become much larger, about 1 μm in width and from 10 μm up to hundreds of micrometers in length. The HFBII fibrils are highly crystalline, showing monoclinic and hexagonal crystal structures as the undried and dried samples, respectively. Importantly, we provided arguments that the HFBII fibrils are probably crystallized from tetrameric aggregates (*15*, *16*). Fibril formation has been observed

† This work was funded by the Academy of Finland (project no. 47465).

* To whom correspondence should be addressed. Phone: +358 9 456 5136. Fax: +358 9 455 2103. E-mail: markus.linder@vtt.fi.

‡ VTT Biotechnology, Technical Research Centre of Finland.

§ Institute of Materials Chemistry, Tampere University of Technology.

|| Department of Physical Sciences, University of Helsinki.

⊥ Department of Physics, Tampere University of Technology.

Department of Engineering, Physics, and Mathematics, Helsinki University of Technology.

10.1021/bi034031t CCC: $25.00
Published on Web 04/18/2003

previously also for other class II hydrophobins, but the role of this phenomenon for the fungal physiology is not known (*17*).

In addition to being biologically interesting, hydrophobins may also show technological promise due to their high surface activity. This surface activity can, as demonstrated for the hydrophobins HFBI and HFBII from *T. reesei*, be seen as extremely high partitioning in surfactant two-phase systems (*14*), which is a method typically used for extracting hydrophobic membrane proteins (*18*). The efficient partitioning allows the use of hydrophobins as purification tags in fusion proteins (*19*). Their adhesion properties are also interesting and allow immobilization of fusion proteins to various surfaces (*20*). More related to the present work, hydrophobins may allow a number of other surface modification techniques, such as arrays or patterning, once their two-dimensional structures on surfaces are known.

Crystalline thin-film formation and nanopatterning is currently attracting much attention because of its implications in several fields (for a review, see ref *21*). In this work, the logic is the following. Hydrophobins are surface-active proteins which form biological surfaces. On the other hand, the progress toward understanding the biological and even technological roles of the organized nanoscopic surface structures, for example, those of S-layer proteins (*22*, *23*), suggested that hydrophobins could offer another platform for nanoscale surface patterns and functionalization. Our attempts to form structured thin films with hydrophobins was also encouraged by the previous observation that in HFBII the actual constituents for the fibrils could be tetrameric shape-persistent supramolecules (*15*). In this work, we produced molecular layers of hydrophobins using the Langmuir−Blodgett (LB)[1] technique and studied them by atomic force microscopy (AFM). It was shown that highly ordered two-dimensional crystalline nanostructures were formed. To interpret the structures, we additionally combined low-resolution models restored from small-angle X-ray scattering (SAXS) intensity data from the hydrophobin solutions as well as wide-angle X-ray data from self-assembled fibrils (*15*). This work represents the most detailed structural study of hydrophobin surface films so far.

MATERIALS AND METHODS

Protein Production and Purification. HFBII was produced using the *T. reesei* strain VTT D-99745 that overproduces HFBII. Bioreactor cultivations were done as described in ref *24*. One liter of the culture supernatant was centrifuged at 4000*g* for 20 min and the pellet discarded. To the supernatant was added 2 g of Berol 325 (Akzo Nobel). After gentle mixing, the solution was allowed to settle in a separation funnel, where the Berol phase was separated. Aliqouots of 100 mL of acetate buffer (50 mM, pH 5.0) and 15 mL of isobutanol were added to the Berol phase, and the mixture was centrifuged for 15 min at 3220*g*. The lower phase was purified further by preparative reversed-phase chromatography using a Vydac C4 (1 × 20 cm) column and a gradient elution from 0.1% trifluoroacetic acid to 100% acetonitrile containing 0.1% trifluoroacetic acid. The peak fractions were pooled and lyophilized.

[1] Abbreviations: LB, Langmuir−Blodgett; AFM, atomic force microscopy; SAXS, small-angle X-ray scattering.

HFBI was produced using the *T. reesei* strain VTT D-98692 in a bioreactor and purified essentially as described in refs *14* and *25*. Mycelium was collected by centrifugation at 3220*g* for 20 min. The 30-mL pellet was suspended in 200 mL of 2% sodium dodecyl sulfate−0.2 M sodium acetate, pH 5, and homogenized with a Polytron (Kinematica) homogenizer. Extraction was continued for 3 h, and then a similar centrifugation was performed and the pellet discarded. Sodium dodecyl sulfate was removed from the remaining supernatant by adding 13 g of anion exchanger AG 2-X8 (Bio-Rad) to 27 mL of solution. Berol extraction, preparative chromatography, and lyophilization were then performed as above.

Langmuir−Blodgett Films. The LB films were prepared using a KSV minitrough LB system (KSV Instruments) using 1 mM acetate buffer, pH 5.0, and 18.0 ± 0.5 °C for the subphase. Analytical-grade chemicals and Milli-Q (Millipore) water were used. Lyophilized HFBI and HFBII were dissolved in water to a concentration of 0.2 mg/mL and spread on the subphase. The surface pressure was recorded at constant trough area as a function of time after 300 μL of the protein solution was spread at the air−water interface. For HFBI, the equilibrium surface pressure value of 0.24 mN/m was reached in 8 min, whereas for HFBII 16 min was required to reach the equilibrium surface pressure value of 1.4 mN/m. Compression of the monolayer was started after the surface pressure had stabilized, 10 and 20 min for HFBI and HFBII, respectively. Surface pressure was measured using a platinum Wilhelmy plate attached to a sensitive balance with an accuracy of ±0.01 mN/m. The monolayers were compressed at a rate of 8.9 Å^2 molecule/min to the deposition pressure of 30 mN/m. The films were transferred onto mica substrates by the vertical lifting method at a rate of 10 mm/min, with transfer ratios near unity.

Atomic Force Microscopy. Mica substrates (sizes 1 × 1 cm^2), covered by the protein LB films, were attached onto steel supports with double-sided tape (Scotch). A NanoScopeIIIa multimode AFM (Digital Instruments, Santa Barbara, CA) equipped with an "E" scanner was used in all measurements. Calibration was performed using a 1 × 1 μm^2 calibration grid (Digital Instruments) for the *x* and *y* directions and 180-nm height standard (Digital Instruments) and gold spheres (Ted Pella, Redding, CA) of 5 nm in diameter for the *z* direction. Images were acquired in ambient conditions. Noncontact silicon cantilevers (NCH, NanoSensors) with the nominal resonance frequency around 300 kHz and tip radius better than 10 nm were used. The tapping mode was used with scan rates 0.6−1 Hz and as low a force as possible, the ratio of set-point amplitude (A_{sp}) and free amplitude (A_f) being 0.75−0.85. For image analysis, a NanoScopeIII offline workstation and a scanning probe image processor (SPIP, Image Metrology, Denmark) were used. The image-processing step included only flattening of all acquired images in order to remove possible tilt in the image data. Imaging of HFBI and HFBII surfaces was reproducible, as similar structures were recorded on several different areas on two separate sample surfaces of both protein films. Imaging in liquid was also attempted but was abandoned due to contamination of the tip by loose hydrated proteins.

Solution SAXS. SAXS experiments were performed using a sealed Cu anode X-ray tube with CuKα radiation (λ =

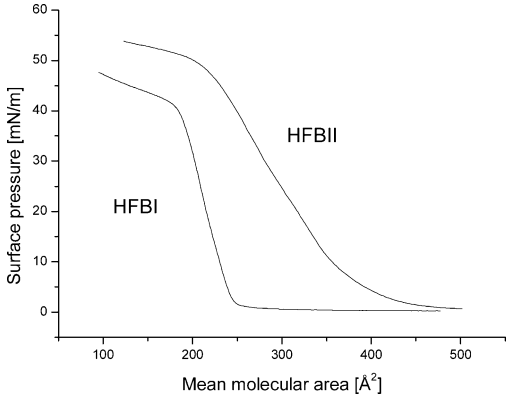

FIGURE 1: Surface pressure−area isotherms of class II hydrophobins HFBI and HFBII at the air−water interface.

1.542 Å), which was monochromatized with a Ni filter and a glass mirror and measured with either a one-dimensional (M-Braun OED-50) or a two-dimensional (Hi Star) proportional counter. The measured range of k values was 0.03−0.5 Å^{-1}, where the length of the scattering vector is defined by $k = (4\pi/\lambda)\sin\theta$, where 2θ is the scattering angle. The background due to the solvent was measured separately and subtracted from the intensity curves of the samples. Further details of the experiments and data analysis are given in ref *15*. Solution SAXS was performed for both HFBI and HFBII at concentrations of 10 and 100 mg/mL.

RESULTS

Interfacial Film Formation. The pressure−area isotherms are shown in Figure 1. HFBII shows a smooth rise of the surface pressure, characteristic for a liquid-expanded phase, and a collapse point near 50 mN/m. The HFBI isotherm is steeper, as characteristic for a liquid-condensed phase, and the collapse point is lower, near 40 mN/m. The limiting areas extrapolated to zero pressure differ considerably, being 258 Å^2 for HFBI and 387 Å^2 for HFBII. This is unexpected since the molecular weights, 7532 for HFBI and 7188 for HFBII, do not differ very much.

In repeated compression−expansion cycles, especially for HFBI, the onset of the second compression curve was shifted to lower molecular areas, but no further changes were observed in the third cycle (see Figure 2). This suggests that aggregates are formed upon the first compression that do not disassemble upon consecutive expansion. This qualitatively supports the hypothesis that the structural entities forming the two-dimensional crystallites could be tetrameric supramolecules, to be discussed later in detail. The reproducibility upon further cycling indicates that once the equilibrium was established during the stabilization after spreading, no molecules were lost to the subphase during compressions. All results were repeatable, but it was noted that some batches of HFBI that contained impurities gave compression curves that were shifted toward smaller mean molecular areas. Despite such variation, the arrayed structures described below were indistinguishable from batch to batch.

AFM Images. LB films of both HFBI and HFBII show polycrystalline structures consisting of two-dimensional oblique single-crystalline domains (see Figure 3A,B). The crystallinity of the protein layer was confirmed using Fourier transformations of the image data (Figure 3C,D), giving the lattice constants $a = 59.2$ Å, $b = 49.9$ Å, $\gamma = 118.9°$ and $a = 58.7$ Å, $b = 44.1$ Å, $\gamma = 122.6°$ for HFBI and HFBII, respectively. There is a slight distortion observed in the AFM images, and hence in the transformed images also, due to scanner hysteresis, creep, and drift in microscope. These phenomena need to be considered here, because relatively slow scan speeds were used and images of the first full scan were captured in order to obtain images of the soft protein surfaces with a noncontaminated tip. HFBI allowed higher resolution images than HFBII, which may indicate that the very surface of the LB film of HFBII on mica is more hydrophilic than that of HFBI, as the thin water layer that exists on every surface under ambient conditions has a significant effect on the tip−surface interaction when both surfaces are hydrophilic. It is obvious that the lateral resolution achieved in the AFM images is higher than expected, given the nominal tip radius of ca. 10 nm. The high resolution could be explained by a possible "micro roughness" of the tip surface, resulting in a much smaller part on the end of the tip actually scanning the surface.

In images covering larger areas (images shown in Supporting Information), the most distinct differences between HFBI and HFBII were in the sizes of the single-crystalline domains and the extent of surface coverage. HFBI typically formed small single-crystalline domains on mica, and the regions between them were very flat, being probably plain mica surface. The average thickness of the single-crystalline domains as compared to the flat surface between them was 13 ± 2 Å. This corresponds to a monolayer thickness (to be discussed later). By contrast, HFBII seemed to cover the

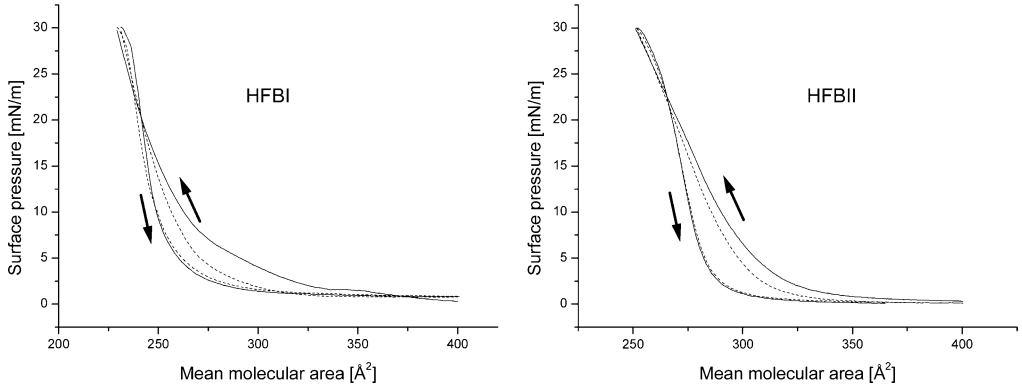

FIGURE 2: Compression−expansion cycles for HFBI and HFBII. Solid and dashed lines are for the first and second cycles, respectively. Lines on the right represent compression and those on the left expansion, as indicated by the arrows. Additional cycles did not differ from the second one (data not shown).

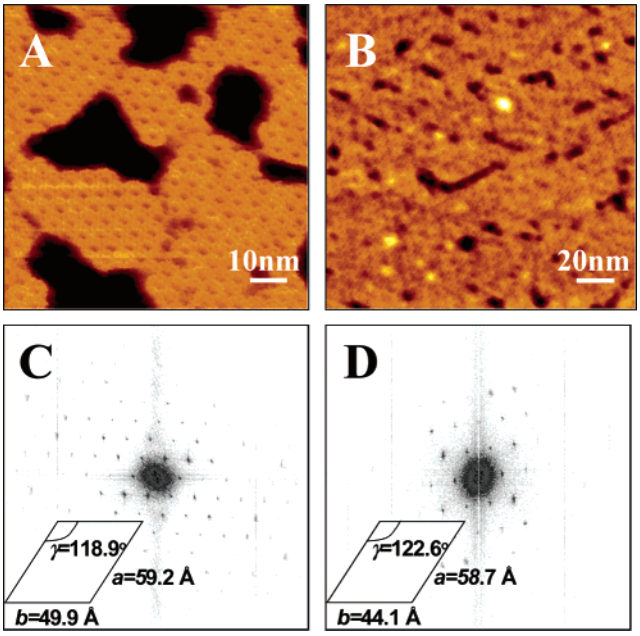

FIGURE 3: AFM topography images of class II hydrophobin LB films on mica. (A) HFBI; image size is 100 × 100 nm^2 and height scale 2 nm. (B) HFBII; image size is 200 × 200 nm^2 and height scale 2 nm. The power spectra and the corresponding crystalline oblique unit cells in real space are shown for (C) HFBI and (D) HFBII. The spectra show that both films have a very high crystallinity despite a higher noise level in the HFBII films.

whole surface more easily, but it had amorphous regions between the single-crystalline domains. In this case, the heights of the domains could not be readily evaluated.

SAXS in the Aqueous Solutions. The SAXS intensities of both HFBI and HFBII at low concentrations of 10 mg/mL obeyed the Guinier law, $I(k) \approx \exp(-^1/_3 k^2 R_g^2)$, at small magnitudes of the scattering vector k, leading to the radius of gyration $R_g \cong 24$ Å for the dissolved entities (*15*). In the same work, the maximum dimensions of the dissolved entities based on SAXS were determined to be 65 Å for both HFBI and HFBII. At 100 mg/mL, the intensity curves showed features arising from a large concentration of proteins. Notably, the intensity curves did not show an upturn toward 0 k, which could arise from larger aggregates of hydrophobin. The results indicate that both HFBI and HFBII are tetramers also at a high concentration of 100 mg/mL. This, along with the supporting observation in size exclusion chromatography (*15*), points toward stability of well-defined supramolecules consisting of four protein chains.

The potential shape of the dissolved tetrameric supramolecules can be restored using the program DAMMIN (*26*). The program builds the scattering units from dummy particles, and simulated annealing is employed to find a configuration that best fits to the SAXS intensity curve. The method was applied for HFBI at the concentration 10 mg/mL for the range $0.02 < k < 0.3$ Å^{-1} and allowed a good fit, with a root-mean square deviation from the experimental data of 5.2 (data not shown). Accordingly, the dissolved entities HFBI (Figure 4A) have a shape resembling a torus, with a diameter of about 65 Å and a thickness of 15 Å. The size agrees with a tetrameric supramolecule, as a crude random walk model (see, for example, ref *27*) suggests one chain to have a diameter of the order of 16 Å. The thickness of the HFBI torus agrees nicely with the height of the monolayer determined by AFM. For comparison, in the case of HFBII, the previously suggested shape of the dissolved entities is depicted in Figure 4B (*15*), showing a four-armed structure which could be a direct consequence of the aggregation of the four chains into a tetramer. Although the approximate sizes of the HFBI and HFBII tetramers are approximately similar, the shapes are clearly different.

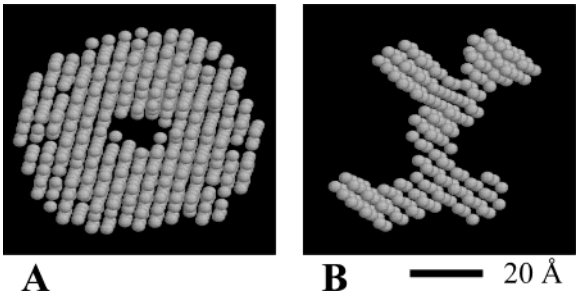

FIGURE 4: Shapes of the dissolved tetramers based on solution SAXS using the program DAMMIN. (A) The torus-shaped supramolecule of HFBI. (B) The four-armed-shaped supramolecule of HFBII. The size of the unit spheres is 2.5 Å, and the largest diameter of the tetramer is 65 Å.

DISCUSSION

The primary experimental observation of this work is that LB films of both HFBI and HFBII form protein arrays with well-defined nanoscopic structures not previously shown for hydrophobins. We will next provide arguments that the structures, in fact, comprise a hierarchical assembly, the first level consisting of tetrameric supramolecules which, on the next level, pack into crystalline arrays. We will also suggest that the thickness of the layer probably corresponds to a monomolecular layer. The two-dimensional crystalline structures are qualitatively similar for both hydrophobins, but high-resolution AFM images revealed that there is a structural difference at the molecular level which might be explained by the different packing constraints of the supramolecules.

The AFM images of HFBI (Figure 3A) show crystalline domains with a regular arrangement of holes or depressions. Furthermore, the edges of these domains run through the depressions in two preferential directions (e.g., in Figure 3A, either horizontal or tilted ca. 30° counterclockwise from vertical), which suggests that the basic building block is the shape of a parallelogram. The size of this indivisible unit is about 50−60 Å, which qualitatively equals the dimensions of the tetramers formed in solution, as determined above using SAXS. The thickness of the HFBI tetramers obtained from the solution SAXS data is about 15 Å, which agrees with the thickness of the monolayer, 13 ± 2 Å, obtained by AFM. Such observations encouraged us to study in more detail whether the packing of the tetrameric supramolecules observed in solutions (Figure 4) could lead to the observed crystalline structures of the LB films, as observed using AFM (Figure 3).

Therefore, an effort was first made to further improve the resolution of the AFM images to the level of ca. 2.5 Å by averaging over several unit cells. This begins by selecting a single crystalline domain, which is visually divided into unit cells. The domains consisted of 50−200 and 200−300 unit cells for HFBI and HFBII, respectively. In the case of HFB II, the image needed to be filtered to bring out the periodic structure because of undue noise in the AFM image (Figure

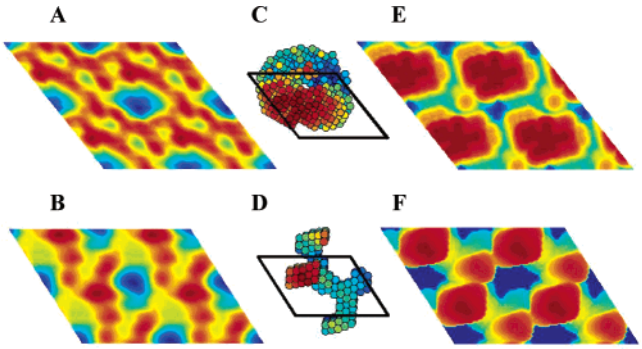

FIGURE 5: Averaged unit cell structures based on averaging over several unit cells of AFM images within the single-crystalline domains for (A) HFBI and (B) HFBII. The color coding of the tetramer models of HFBI (C) and HFBII (D) obtained from solution SAXS data. The putative arrangement of hydrophobin tetramers in the protein layer, a reconstructed AFM image based on the tetramer model for HFBI (E) and HFBII (F).

3B). For this, a multiple band-pass filter centered at the reciprocal lattice points (Figure 3D) was used (*28*). After the unit cell was identified, an average of the height profile within the unit cell was calculated to the aforementioned 2.5 Å precision. In both cases, several domains of the original image were tried, all of which gave essentially the same result.

The enhanced resolution images showing 2 × 2 unit cells are depicted in Figure 5A,B for HFBI and HFBII, respectively. Next, the entities corresponding to the dissolved tetramers of HFBI (Figure 5C) and HFBII (Figure 5D) were arranged to provide the best geometrical packing of the surface. The obtained assemblies were convoluted using a ca. 1 nm "tip" (Figure 5E,F) to better compare with the structure obtained from the AFM images. Comparison of parts B and F of Figure 5 suggests that, for HFBII, we are able to explain the features and dimensions of the crystalline structures observed by the AFM images in terms of packing of the solution tetrameric supramolecules in some detail. The corresponding analysis for HFBI is less satisfactory, as it is able to explain the overall dimensions but is less accurate in the details. Such differences may indicate that the conformations of the proteins are not the same in the 2D films and the aqueous solution. In addition, the hydrophobic mica substrate and the buffer may also deform the 2D structure, as observed with streptavidin, showing two different 2D structures from two buffered solutions (*29*).

The present data thus suggest that we should consider the role of tetrameric or smaller aggregates to obtain a better understanding of the surface activity and phase behavior of hydrophobins. Solution SAXS data presented in this work and previously (*15*) show that both HFBI and HFBII exist as tetramers in solution. No further levels of aggregation or self-assembly occurred spontaneously in solution, even at concentrations as high as 100 mg/mL. On the other hand, at lower concentrations of protein (below 0.5 mg/mL), there is an equilibrium between monomers and dimers, as concluded from the behavior of samples run on gel filtration columns.

Differences in tetramer structure and ultrastructure in surface films could provide an explanation for the different aggregation properties and biological roles observed for HFBI and HFBII (*30*, *31*). There is also an indication of stronger lateral interactions in the HFBI film, which causes hysteresis in sequential compression cycles. In *T. reesei*, the hydrophobins are regulated very differently: HFBI is induced by starvation or glucose, whereas HFBII is regulated in a manner similar to that of the cellulase genes, in the presence of the fungus natural substrate, cellulose. HFBI seems to stick to the mycelium much more tightly than HFBII, suggesting possible interactions with other cell wall components. Although HFBII is also found as coatings on spores, it is mainly found secreted into the surrounding medium. Mixing of HFBI and especially HFBII samples rapidly produces aggregates, which for HFBII has been shown to be highly crystalline (*15*, *16*). A possible mechanism is that assemblages formed at the air interface associate or compress into larger bundles that precipitate during mixing. The differences in film ultrastructures could lead to differences in the tendency for filbrils to form and in the stability of fibrils, as has been observed.

In summary, we have shown that highly surface-active proteins of class II hydrophobins HFBI and HFBII form well-defined two-dimensional crystalline surface layers in LB films. On the basis of detailed analysis of the AFM images and combination of SAXS data on solutions of HFBI and HFBII, we suggest that the structure formation is in fact hierarchical, where four protein chains first form tetrameric supramolecules, which further pack into crystalline domains. We suggest a torus-like shape for the HFBI tetramers and a four-armed shape for the HFBII tetramers. Hydrophobins could offer new options for surface modification and nanostructured functional surfaces once the assembly processes and the structural hierarchy, as well as their effects on adhesion and surface activity, can be controlled at the molecular level. This brings the interest in hydrophobins beyond fungal physiology and into the field of nanostructured materials.

ACKNOWLEDGMENT

Riitta Suihkonen is thanked for technical assistance and Dr. Jouko Peltonen is thanked for fruitful discussions.

SUPPORTING INFORMATION AVAILABLE

Lower magnification AFM images of HFBI and HFBII. This material is available free of charge via the Internet at http://pubs.acs.org.

REFERENCES

1. Kershaw, M. J., and Talbot, N. J. (1998) *Fungal Genet. Biol. 23*, 18−33.
2. Wösten, H. A., and de Vocht, M. L. (2000) *Biochim. Biophys. Acta 1469*, 79−86.
3. Wösten, H. A., van Wetter, M. A., Lugones, L. G., van der Mei, H. C., Busscher, H. J., and Wessels, J. G. (1999) *Curr. Biol. 9*, 85−88.
4. Talbot, N. J. (1999) *Nature 398*, 295−296.
5. Ebbole, D. J. (1997) *Trends Microbiol. 5*, 405−408.
6. Yaguchi, M., Puszari-Carey, M., Roy, C., Surewicz, W. K., Carey, P. R., Stevenson, K. J., Richards, W. C., and Takai, S. (1993) in *Dutch Elm Disease Research, Cellular and Molecular Approaches* (Sticklen, M. B., and Sherald, J. L., Eds.) pp 152−170, Springer-Verlag, New York.
7. Wessels, J. G. H. (1994) *Annu. Rev. Phytopathol. 32*, 413−437.
8. Scholtmeijer, K., Janssen, M. I., Gerssen, B., de Vocht, M. L., van Leeuwen, B. M., van Kooten, T. G., Wosten, H. A., and Wessels, J. G. (2002) *Appl. Environ. Microbiol. 68*, 1367−1373.

9. de Vocht, M. L., Reviakine, I., Wosten, H. A., Brisson, A., Wessels, J. G., and Robillard, G. T. (2000) *J. Biol. Chem. 275*, 28428−28432.
10. Wösten, H. A. B., de Vries, O. M. H., and Wessels, J. G. H. (1993) *Plant Cell 5*, 1567−1574.
11. Scherrer, S., De Vries, O. M., Dudler, R., Wessels, J. G., and Honegger, R. (2000) *Fungal Genet. Biol. 30*, 81−93.
12. Butko, P., Buford, J. P., Goodwin, J. S., Stroud, P. A., McCormick, C. L., and Cannon, G. C. (2001) *Biochem. Biophys. Res. Commun. 280*, 212−215.
13. Mackay, J. P., Matthews, J. M., Winefield, R. D., Mackay, L. G., Haverkamp, R. G., and Templeton, M. D. (2001) *Structure 9*, 83−91.
14. Linder, M., Selber, K., Nakari-Setälä, T., Qiao, M., Kula, M.-R., and Penttilä, M. (2001) *Biomacromolecules 2*, 511−517.
15. Torkkeli, M., Serimaa, R., Ikkala, O., and Linder, M. (2002) *Biophys. J. 83*, 2240−2247.
16. Serimaa, R., Torkkeli, M., Paananen, A., Linder, M., Kisko, K., Knaapila, M., Ikkala, O., Vuorimaa, E., Lemmetyinen, H., and Seeck, O. (2003) *J. Appl. Crystallogr.* (in press).
17. Takai, S. (1974) *Nature 252*, 124−126.
18. Bordier, C. (1981) *J. Biol. Chem. 256*, 1604−1607.
19. Collen, A., Persson, J., Linder, M., Nakari-Setälä, T., Penttilä, M., Tjerneld, F., and Sivars, U. (2002) *Biochim. Biophys. Acta 1569*, 139−150.
20. Linder, M., Szilvay, G. R., Nakari-Setälä, T., Söderlund, H., and Penttilä, M. (2002) *Protein. Sci. 11*, 2257−2266.
21. Kumenko, I., Rapaport, H., Kjaer, K., Als-Nielsen, J., Weissbuch, I., Lahav, M., and Leiserowitz, L. (2001) *Chem. Rev. 101*, 1659−1696.
22. Sleytr, U. B., Pum, D., and Sara, M. (1997) *Adv. Biophys. 34*, 71−79.
23. Sara, M., and Sleytr, U. B. (2000) *J. Bacteriol. 182*, 859−868.
24. Bailey, M., Askolin, S., Hörhammer, N., Tenkanen, M., Linder, M., Penttilä, M., and Nakari-Setälä, T. (2002) *Appl. Microbiol. Biotechnol. 58*, 721−727.
25. Askolin, S., Nakari-Setälä, T., and Tenkanen, M. (2001) *Appl. Microbiol. Biotechnol. 57*, 124.
26. Svergun, D. I. (1999) *Biophys. J. 76*, 2879−2886.
27. Gedde, U. (1995) *Polymer physics*, Chapman and Hall, London.
28. Dupont, O., Jonas, A. M., Nysten, B., Legras, R., Adriaensens, P., and Gelan, J. (2000) *Macromolecules 33*, 562−568.
29. Lenne, P.-F., Berge, B., Renault, A., Zakti, C., Venien-Bryan, C., Courty, S., Balavoine, F., Bergsma-Schutter, W., Brisson, A., Grubel, G., Boudet, N., Konovalov, O., and Legrand, J-F. (2000) *Biophys. J. 79*, 496−500.
30. Nakari-Setälä, T., Aro, N., Kalkkinen, N., Alatalo, E., and Penttilä, M. (1996) *Eur. J. Biochem. 235*, 248−255.
31. Nakari-Setälä, T., Aro, N., Ilmen, M., Munoz, G., Kalkkinen, N., and Penttilä, M. (1997) *Eur. J. Biochem. 248*, 415−423.

BI034031T